INTERFACE

royalsocietypublishing.org/journal/rsif

Research



Cite this article: Xu Z, Yue P, Feng JJ. 2023 Poroelastic modelling reveals the cooperation between two mechanisms for albuminuria. *J. R. Soc. Interface* **20**: 20220634. https://doi.org/10.1098/rsif.2022.0634

Received: 28 August 2022 Accepted: 8 December 2022

Subject Category:

Life Sciences—Physics interface

Subject Areas:

biomathematics, biomechanics, biophysics

Keywords:

glomerular basement membrane, poroelasticity, filtration, albuminuria, gel compression hypothesis

Author for correspondence:

James J. Feng e-mail: james.feng@ubc.ca

Electronic supplementary material is available online at https://doi.org/10.6084/m9.figshare. c.6350499.

THE ROYAL SOCIETY

Poroelastic modelling reveals the cooperation between two mechanisms for albuminuria

Zelai Xu¹, Pengtao Yue³ and James J. Feng^{1,2}

(D) ZX, 0000-0001-9052-9896; PY, 0000-0001-8343-846X; JJF, 0000-0002-7141-5823

Albuminuria occurs when albumin leaks abnormally into the urine. Its mechanism remains unclear. A gel-compression hypothesis attributes the glomerular barrier to compression of the glomerular basement membrane (GBM) as a gel layer. Loss of podocyte foot processes would allow the gel layer to expand circumferentially, enlarge its pores and leak albumin into the urine. To test this hypothesis, we develop a poroelastic model of the GBM. It predicts GBM compression in healthy glomerulus and GBM expansion in the diseased state, essentially confirming the hypothesis. However, by itself, the gel compression and expansion mechanism fails to account for two features of albuminuria: the reduction in filtration flux and the thickening of the GBM. A second mechanism, the constriction of flow area at the slit diaphragm downstream of the GBM, must be included. The cooperation between the two mechanisms produces the amount of increase in GBM porosity expected in vivo in a mutant mouse model, and also captures the two in vivo features of reduced filtration flux and increased GBM thickness. Finally, the model supports the idea that in the healthy glomerulus, gel compression may help maintain a roughly constant filtration flux under varying filtration pressure.

1. Introduction

Albuminuria is a kidney disease with too much of the protein albumin leaking through the kidney into the urine. The function of the kidney relies on microvascular filtration units known as glomeruli (figure 1). Their extraordinary size-selective barrier function can be appreciated from a few numbers. First, a healthy human produces about 1801 of primary urine daily. Based on the protein concentration in the plasma, this much liquid corresponds to about 10 kg of proteins being filtered by the glomeruli per day. Of this amount of proteins, only about 1 g passes the glomerular filtration barrier [1]. That yields a filtration efficiency of 99.99%. Second, even the smallest breach of this barrier can cause severe disease. Lowering the albumin retention rate from 99.9995% to 99.66%, for example, produces 'catastrophic nephrotic syndromes' [2]. Therefore, not only is the glomerulus exceptionally effective in keeping proteins in the blood, its ultrafiltration must also be controlled to exceptional precision. For these reasons, it is important to understand the physical mechanisms underlying glomerular filtration.

For the exquisite size selectivity of the glomerular filtration barrier, a number of explanations have been proposed, and the debates and resulting insights have been summarized by a number of reviews [2–8]. The glomerular filtration barrier consists of three layers, a fenestrated endothelium, a glomerular basement membrane (GBM) and an epithelium of podocytes (figure 1). While all three contribute to the barrier function [3,9–11], accumulating evidence points to the GBM as key to size selectivity [2,7,12–16]. For example, Lawrence *et al.* [15] observed experimentally that injected nanoparticles

¹Department of Chemical and Biological Engineering, and ²Department of Mathematics, University of British Columbia, Vancouver, British Columbia, Canada V6T 1Z2

³Department of Mathematics, Virginia Tech, Blacksburg, VA 24061, USA

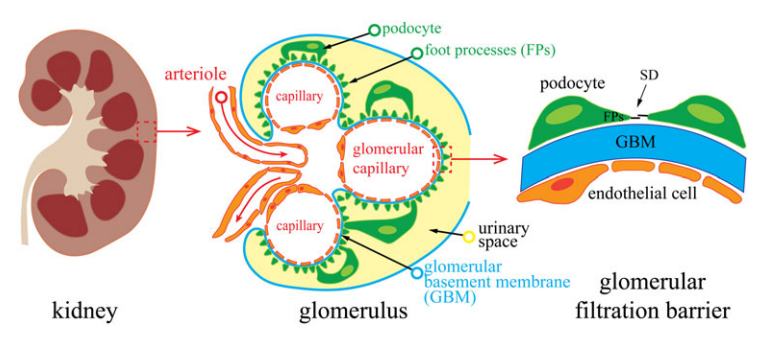


Figure 1. Schematics showing the glomerular filtration barrier in the kidney. Each glomerulus encloses a network of capillaries through which the blood is filtered. The capillary wall consists of a fenestrated endothelium on the inside, a glomerular basement membrane (GBM) and podocytes on the outside. The liquid filtrate passes through the endothelium and the GBM, and flows out through the slit diaphragm (SD) between the foot processes (FPs) of the podocytes into the urinary space.

permeated into the GBM, accumulated upstream of the podocytes, but none appeared upstream of the slit diaphragm (SD). Thus, the question about the mechanism of glomerular filtration takes on a more concrete form: how does the GBM effect precise size selectivity?

The GBM is a dense but porous hydrogel layer with a polymer network consisting of laminins, collagen, nidogens and heparan sulfate proteoglycans [7]. The transport of water and macromolecular solute through the GBM is a multifaceted process, for which several models have been proposed. The two-pore model focuses on steric exclusion of larger macromolecules by pores of different sizes [17,18]. The electrokinetic model hinges on an electrostatic potential that develops across the glomerular barrier during filtration, which drives the negatively charged albumin back into the plasma by electrophoresis [1,19]. These two effects probably coexist and account for much of the sieving effect. But they provide mostly fixed barriers to protein passage, and cannot explain the minute difference in filtration efficiency between a healthy glomerulus and one with albuminuria [2].

The gel permeation and diffusion model assumes that water passes through the pores of the GBM by convection, whereas large protein molecules rely mainly on diffusion [13]. Albuminuria, in this model, would not be due to greater protein transport but to suppressed solvent transport. Although conceptually straightforward, this model predicts outcomes that contradict several experimental observations [2,20,21]. As an alternative, Fissell and others have proposed a gel-compression hypothesis to explain the change of permeability between a healthy GBM and a diseased one [2,6,8,21]. In health, the interdigitating foot processes (FPs) of the podocytes exert an in-plane tension that produces a 'buttressing force' on the outer surface of the GBM thanks to the curvature of the glomerular capillary [2,8,21,22]. This can be likened to surface tension on a curved liquid surface producing a Laplace pressure. Thus the GBM is compressed by the filtration pressure on the endothelial side and the buttressing force on the epithelial side. Its permeability decreases as a result to prevent albumin leakage. In albuminuria, on the other hand, the damaged podocytes and FPs can no longer supply sufficient buttressing force [3,4,9,10,21]. As a result, the GBM changes its mode of deformation from radial compression to circumferential expansion. The expansion dilates the blood vessel and 'rarifies' the subepithelial GBM, enlarging its pores and increasing its permeability to albumin.

Butt *et al.* [21] put the hypothesis to test with healthy and diseased mice, and found four intriguing morphological and hydrodynamic clues to albuminuria:

- (i) Albuminuria strongly correlates with the shortening of the SDs, which contain openings for the efflux of urine downstream of the GBM (figure 1).
- (ii) The glomerular filtration rate (GFR) also decreases in the diseased mice, but by a smaller percentage than the reduction in SD length.
- (iii) The diseased mice show capillary dilatation.
- (iv) The GBM also becomes thicker in the diseased mice.

From (i) and (ii), Butt *et al.* [21] inferred that the hydraulic permeability of the GBM must be increased in the diseased mice, thus providing an *indirect confirmation* of the gel-compression hypothesis. Observation (iii) is consistent with the hypothesized circumferential expansion. However, (iv) is a surprise, as one may expect the circumferential expansion of the GBM to *reduce* its thickness.

This work approaches the problem from the opposite direction to that of Butt *et al.* [21]: we model the poroelastic mechanics of the GBM to see if the known precursors of albuminuria, the weakening buttress and the shortening SD, lead to greater GBM porosity and permeability. The model reveals that such an outcome arises from the cooperation between two mechanisms: the circumferential stretching of the gel due to the loss of the FPs, and the reduction in GFR due to SD constriction. The linkage between the two is that a lower GFR implies a reduced Darcy drag inside the GBM, which then compresses it less severely. Thus, the model is able to explain all the four experimental observations, and, using appropriate parameter values, to predict the correct level of gel porosity that Butt *et al.* [21] have inferred from *in vivo* data.

2. Theoretical formulation and numerical setup

2.1. Physical model

In view of recent studies of the mechanics of basement membranes [23,24], we represent the GBM as a poroelastic gel layer composed of an elastic network and aqueous solvent. Among the three components of the glomerular filtration barrier (figure 1), the endothelium has limited contribution to the size-selective filtration because of its fenestrae [15]. Thus, we omit the endothelial cells and focus on the GBM and the FPs.

Figure 2 depicts a quarter of the glomerular capillary, and the computational domain is an annular sector delineated by the two arcs Γ_1 and Γ_2 , respectively, at $r = 0.9R_0$ and $R_0 + \delta_0$ in the undeformed state, R_0 being the inner radius of the

undeformed GBM and δ_0 its initial thickness. With flow, R and δ will change. The inner arc Γ_1 stays fixed at $0.9R_0$, but the outer arc Γ_2 moves according to $r = R + \delta$. The filtration flow is driven by the pressure difference between P_1 at Γ_1 and P=0 in the urinary space downstream of the FPs. The GFR can be computed from the velocity V_1 at Γ_1 : GFR = $V_1(2\pi \times 0.9R_0)$. Although the blood pressure varies with every heart beat, for our purpose we assume a constant average pressure P_1 . The flow inside the lumen is inertialess Stokes flow along the radial direction, and the exact position of the inner arc Γ_1 is unimportant as long as it is within the lumen. The GBM is a layer of poroelastic gel, with initially constant fluid and solid volume fractions ϕ_{f0} and $\phi_{s0} = 1 - \phi_{f0}$. As the GBM is deformed by the flow, ϕ_f and ϕ_s may vary in time and along the radial direction. The flow is expected to be one dimension along the radial r-direction, and one may start with a one-dimensional setup. But as the computational cost is moderate even in two dimensions, we have adopted a previously developed two-dimensional setup [25] for convenience.

To reflect the morphological changes due to FP effacement, we focus on two features. The first is the weakening of the buttress force on the downstream surface of the GBM [2,8,22]. The second is the effect of shortened and narrowed SD on restricting the filtration flux [21,26,27]. We model the FP buttressing force by elastic springs that resist normal displacement of the GBM's outer surface Γ_2 with a radial normal stress

$$\tau_2 = Eu_2, \tag{2.1}$$

where E is an elastic coefficient and u_2 is the radial displacement of the outer boundary Γ_2 . This will be implemented in boundary conditions on Γ_2 . Note that we take τ_2 to be positive even though it is a compressive stress.

After passing through the GBM, the filtrate flows through the SD into the urinary space, where the pressure can be set to P = 0 without loss of generality. The viscous flow across the SD requires a pressure drop

$$P_2 = \mu_D V_2, \tag{2.2}$$

where P_2 and V_2 are, respectively, the fluid pressure and velocity on Γ_2 , just outside GBM, and μ_D is a friction coefficient characterizing the resistance to the fluid downstream of the GBM. As will be seen later, μ_D allows us to account for the flow restricting effect of shortened and narrowed SDs in albuminuria.

2.2. Governing equations and boundary conditions

In our context, the flow in the lumen is of little interest, so we treat the blood as a Newtonian fluid of viscosity μ_b undergoing inertialess flow, despite its non-Newtonian rheology [28]. Its flow is governed by

$$\nabla \cdot \mathbf{V} = 0 \tag{2.3}$$

and

$$\nabla P - \mu_h \nabla^2 \mathbf{V} = 0, \tag{2.4}$$

in which V and P denote the velocity and pressure, respectively.

The GBM is an elastic porous medium that can be described by the poroelastic theory. It consists of a fluid phase (volume fraction ϕ_f) and a solid phase (volume fraction

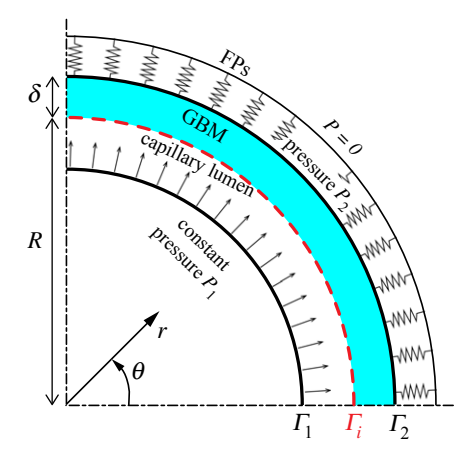


Figure 2. The computational domain is between the arcs Γ_1 and Γ_2 . The red dashed line Γ_i represents the interface between the blood in the capillary lumen and the GBM. The filtration is driven by a constant pressure P_1 on Γ_1 and the flow direction is indicated by the array of arrows. The buttressing effect of the FPs is represented by elastic springs pushing on the exit of the domain Γ_2 . With symmetry conditions imposed on the two radial boundaries $\theta=0$ and $\theta=\pi/2$, the flow is one dimension in the r-direction.

 $\phi_s = 1 - \phi_f$). The continuity of each phase dictates the evolution of its volume fraction:

$$\frac{\partial \phi_f}{\partial t} + \nabla \cdot (\phi_f \mathbf{v}_f) = 0 \tag{2.5}$$

and

$$\frac{\partial \phi_s}{\partial t} + \nabla \cdot (\phi_s \mathbf{v}_s) = 0, \tag{2.6}$$

where \mathbf{v}_f and \mathbf{v}_s are the intrinsic phase-averaged fluid and solid velocities. The motion of each phase is governed by a force balance:

$$\nabla \cdot (\phi_f \sigma_f) - \phi_f \nabla p + \mathcal{F}^{s \to f} = 0$$
 (2.7)

and

$$\nabla \cdot (\phi_{c} \sigma_{s}) - \phi_{c} \nabla p + \mathcal{F}^{f \to s} = 0, \tag{2.8}$$

where σ_f and σ_s are the stress tensor for the fluid and solid phase, respectively, and p is the pressure inside the basement membrane. The Brinkman stress of the fluid phase is $\sigma_f = \mu [\nabla \mathbf{v}_f + (\nabla \mathbf{v}_f)^T]$, μ being the viscosity of the filtrate, i.e. the pore fluid in the GBM. The solid velocity \mathbf{v}_s is the material derivative of the solid displacement \mathbf{u}_s : $\mathbf{v}_s = D\mathbf{u}_s/Dt$, and \mathbf{u}_s determines the solid stress tensor according to the neo-Hookean model:

$$\boldsymbol{\sigma}_s = \mu_s J^{-1}(\mathbf{F}\mathbf{F}^T - \mathbf{I}) + \lambda_s (J - 1), \tag{2.9}$$

where μ_s and λ_s are the Lamé constants, $\mathbf{F} = \hat{\nabla} \mathbf{u}_s$ is the deformation gradient tensor and $J = |\mathbf{F}|$. The gradient $\hat{\nabla}$ is computed in the Lagrangian frame attached to the solid phase [25]. Finally, the Darcy drag $\mathcal{F}^{s \to f}$ or $\mathcal{F}^{f \to s}$ between the fluid and solid phase is given by

$$\mathcal{F}^{s \to f} = -\mathcal{F}^{f \to s} = \xi \phi_f \phi_s (\mathbf{v}_s - \mathbf{v}_f), \tag{2.10}$$

where the drag coefficient ξ is related to the Darcy permeability k: $\xi = \mu \phi_f/(k\phi_s)$. For realistic parameters, the results will show that the viscous stresses in the lumen (equation (2.4)) and in the pores (equation (2.7)) are both negligible relative to the Darcy drag.

With symmetry conditions imposed on the two radial boundaries of the computational domain (figure 2), the flow is essentially one dimension along the r-direction. On the inner surface Γ_i of the GBM, we imposed the boundary conditions BC2 developed in our earlier work [29]:

$$\mathbf{V} \cdot \mathbf{n} = (\phi_s \mathbf{v}_s + \phi_f \mathbf{v}_f) \cdot \mathbf{n}, \qquad (2.11)$$
$$(\mathbf{\Sigma} - P\mathbf{I}) \cdot \mathbf{n} = (\phi_s \boldsymbol{\sigma}_s + \phi_f \boldsymbol{\sigma}_f - p\mathbf{I}) \cdot \mathbf{n}, \qquad (2.12)$$

$$(\mathbf{Z} - P\mathbf{I}) \cdot \mathbf{n} = (\phi_s \boldsymbol{\sigma}_s + \phi_f \boldsymbol{\sigma}_f - p\mathbf{I}) \cdot \mathbf{n}, \tag{2.12}$$

$$(\mathbf{V} - \mathbf{v}_f) \cdot \mathbf{n} = \eta \mathbf{n} \cdot [(\mathbf{\Sigma} - P\mathbf{I}) - (\boldsymbol{\sigma}_s - p\mathbf{I})] \cdot \mathbf{n}, \tag{2.13}$$

$$(\mathbf{V} - \mathbf{v}_f) \cdot \mathbf{t} = \beta \mathbf{n} \cdot \mathbf{\Sigma} \cdot \mathbf{t} \tag{2.14}$$

$$\phi_s(\mathbf{v}_s - \mathbf{v}_f) \cdot \mathbf{t} = -\beta \mathbf{n} \cdot \boldsymbol{\sigma}_s \mathbf{t}, \tag{2.15}$$

where \mathbf{n} is the outward unit normal vector on the hydrogel surface. The first two conditions enforce mass and traction balance across the fluid-gel interface, while the last three express the normal and tangential velocity jumps in terms of stress jumps. In our radially one-dimensional flow, the tangential velocity conditions are irrelevant. They are retained formally because the flow setup is nominally two dimensions (figure 2).

As noted earlier, a constant pressure P_1 is imposed on the entry to the computation domain Γ_1 . On the exit Γ_2 , the boundary conditions should account for the buttressing stress τ_2 from the FPs. The normal traction balance is rewritten as

$$(\mathbf{\Sigma} - P\mathbf{I}) \cdot \mathbf{n} - \tau_2 \mathbf{n} = (\phi_s \boldsymbol{\sigma}_s + \phi_f \boldsymbol{\sigma}_f - p\mathbf{I}) \cdot \mathbf{n}. \tag{2.16}$$

To complete the mathematical setup, we need a normal velocity jump condition on Γ_2 , which is derived using the normal traction balance above in the electronic supplementary material:

$$(\mathbf{V} - \mathbf{v}_f) \cdot \mathbf{n} = \eta \mathbf{n} \cdot [(\mathbf{\Sigma} - P\mathbf{I}) - (\boldsymbol{\sigma}_s - p\mathbf{I})] \cdot \mathbf{n} - \eta \frac{\tau_2}{\phi_s} \mathbf{n}, \quad (2.17)$$

where the pressure P_2 is related to the filtration flux or V_2 via

Thus set up, the mathematical problem is solved by finite elements with an arbitrary Lagrangian-Eulerian scheme to track the movement of the fluid-GBM interface. The two-dimensional computational domain is meshed by quadrilateral elements, with bilinear Q1 discretization for the pressures, and quadratic Q2 discretization for the velocities, stresses and the volume fractions. The code is developed using the open-source finite-element library deal.II [30], and algorithmic details can be found in [25].

2.3. Parameter estimation

Table 1 summarizes all the parameters of our model. Their evaluation makes maximum use of available information in the literature, and for some only rough ranges can be determined. Details of the parameter evaluation are given in the electronic supplementary material, and in the following we elaborate on the two most important parameters for testing albuminuria, E and μ_D , whose estimation is also the most

The change from the healthy to the diseased glomerulus is modelled in part by reduction of the elastic modulus E for the buttressing force (equation (2.1)). However, the physical origin of the buttressing force is not so much the rigidity of the podocytes as the in-plane tension generated by the interdigitated FPs (cf. fig. 1 of [8]). No quantitation of such tension seems to be available in the literature, and we have

Table 1. Values of model parameters and their sources.

parameters	approximate values
initial capillary radius R_0	7 μm [31]
initial GBM thickness δ_0	0.3 μm [13]
initial solid fraction ϕ_{s0}	0.075 [13,21]
filtration pressure P ₁	5.3 kPa [8]
blood viscosity μ_b	4×10^{-3} Pa s [32]
filtrate viscosity μ	10 ⁻³ Pa s [33,34]
permeation coefficient η	$2.7 \times 10^{-5} \ \mu m \ (Pa \ s)^{-1} \ [21]$
Lamé parameter μ_s	20 kPa [35]
Lamé parameter λ_{s}	20 kPa [35]
Darcy drag coefficient ξ	10 ⁴ Pa s μm ⁻² [23,36]
FP elastic coefficient <i>E</i>	healthy: 286 kPa μ m $^{-1}$
	diseased: 2.57 kPa μ m $^{-1}$
FP viscous coefficient μ_D	healthy: 147 Pa s µm ⁻¹
	diseased: 588 Pa s μm ^{—1}

to determine E by alternative means. For the healthy state, we choose a large enough $E = 286 \text{ kPa} \,\mu\text{m}^{-1}$ such that the FPs are essentially rigid against the filtration pressure. This particular value comes from a dimensionless modulus $\bar{E} = ER_0/\mu_s = 100$, the numerical experimentation having been carried out in dimensionless variables. For the diseased state, we have tested a range of softened E values, and found that $E = 2.57 \text{ kPa } \mu\text{m}^{-1}$ would yield 13% of capillary dilatation, the observed amount in Butt's experiments for the diseased glomerulus [21]. Thus, the softened E for the diseased state is chosen by fitting.

The parameter μ_D is key to modelling the filtration flow (equation (2.2)). It depends on the complex flow geometry downstream of the GBM, especially that of the SD, schematically shown in figure 3, adapted from Rodewald & Karnovsky [37]. More recent, higher-resolution imaging has revealed variations in SD shape and size [38,39]. For simplicity, however, we will adopt the rectangular pore shape and the dimensions of Rodewald & Karnovsky [37]. The fluid flows through the pores framed by the cross strands, the central filament and the edge of the FP, and the primary source of dissipation is viscous friction in the narrow passage. The pore has width w = 14 nm, height h = 4 nm and a depth that equals the thickness of the cross strands: d = 7 nm [27]. As w far exceeds h, we assume planar Poiseuille flow with a parabolic profile in the h-direction, and relate the pressure drop P_2 across the SD to the flux through each pore Q_{pore} by

$$P_2 = \frac{12\mu Q_{\text{pore}}}{wh^3} \cdot d. \tag{2.18}$$

Note that we have set the pressure outside the SD to zero.

The volume flux Q_{pore} can be estimated from the total fluid flux V_2S , S being the flow area at Γ_2 , and the number of pores. The number of pores is N=2L/H, L being the total SD length over the area S and H = 11 nm being the height of each repeating unit of cross strands, the factor of 2 accounting for the two columns of pores in the SD. Thus, the pressure P_2 can be related to the velocity V_2 , and we

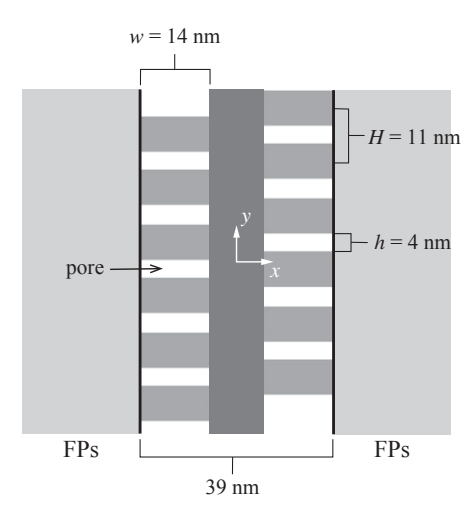


Figure 3. The SD consists of a central filament and two columns of cross strands that bridge the central filament and each of the two apposed FP cell membranes [37]. The fluid flows through the rectangular pores (in the *z*-direction into the page) between the cross strands.

obtain from equation (2.2)

$$\mu_D = \frac{6\mu dH}{wh^3} \frac{S}{L}. \tag{2.19}$$

Butt et~al.~[21] measured the SD length per unit area as $L/S=3.5~\mu m^{-1}$ for the healthy glomerulus. This gives us $\mu_D=147~{\rm Pa~s~\mu m^{-1}}$ in health. FP effacement reduces the SD length by 50–63% [21] while the SD width narrows from 39 nm to 15–20 nm [27]. Thus, L and w are each reduced roughly by a factor of 2, and the flow area at the SD is constricted by a factor close to 4. Accordingly, we take $\mu_D=588~{\rm Pa~s~\mu m^{-1}}$ for the diseased state. A higher μ_D would reduce the flow rate through the filtration barrier, and its effect on the configuration of the GBM will be explored in conjunction with that of a weakened buttressing force.

3. Results

Downloaded from https://royalsocietypublishing.org/ on 28 August 2023

We focus on the solid fraction of the GBM as it determines the permeability and the risk for albuminuria. A higher solid fraction means that the GBM is denser and less permeable. We first present results for the healthy glomerulus where the FPs can provide enough buttressing force. Then we investigate the effect of FP injury by varying the buttressing modulus E of equation (2.1) and the viscous friction coefficient μ_D of equation (2.2).

3.1. The healthy state

Our simulation starts from an initial condition with a uniform GBM of solid fraction ϕ_{s0} = 0.075 everywhere. The filtration pressure P_1 drives an outward radial flow. As a result, the GBM is compressed by the pressure and flow, and the capillary may dilate slightly. We are interested only in the steady state.

The numerical results, obtained with the parameters of table 1 for the healthy glomerulus, allow us to verify directly the concept of gel compression [6,12]. Figure 4a depicts the gel compression due to the filtration flow. The inset shows that while the outer surface of the GBM has expanded slightly (from r = 7.35 to $7.36 \,\mu\text{m}$), its inner surface has been compressed considerably (from r = 7 to $7.11 \,\mu\text{m}$). Thanks to

the relatively rigid buttressing, the FPs have effectively restrained the dilatation of the capillary. The colour contours confirm the elevated solid fraction ϕ_s . The $\phi_s(r)$ profile is compared before and after the compression in figure 4b. The compression yields a roughly linear $\phi_s(r)$ profile, with an average $\bar{\phi}_s = 0.10$, a 33% increase over the initial value of $\phi_{s0} = 0.075$.

We further explore the gel compression from the pressure and flow profiles across the GBM (figure 5). The blood inside the lumen experiences little viscous dissipation. Thus, $P(r) \approx P_1$ is essentially a constant. The velocity V(r) decreases with r because of the requirement of volume conservation in the radial flow geometry: $\partial(V r)/\partial r = 0$. Upon entering the GBM, the pressure suffers an abrupt drop that, according to equation (2.12), serves to counter the solid and fluid normal stresses inside the gel. For our low viscosity μ , the viscous normal stress is small. Thus, most of the pressure drop is expended on σ_s , compressing the GBM and elevating ϕ_s from 0.075 to 0.094 at the upstream interface (figure 4b). Meanwhile, the velocity jumps up suddenly as required by mass conservation of equation (2.11).

Inside the gel, p(r) continues to drop at a sharp slope because of the Darcy drag exerted by the fluid flow on the polymer network. Since this drag is distributed along the GBM's thickness, the gel suffers cumulative compression further downstream. This explains the gradual increase of ϕ_s with r in figure 4b. As the solid compacts the pore space, volume conservation tends to raise the pore velocity $v_f(r)$. Thus, $v_f(r)$ declines more gently inside the GBM than V(r) does upstream of the gel, which is dictated by the radial geometry. Finally, upon exiting the GBM, the pressure suffers another drop to $P_2 = 0.463$ kPa while the velocity drops to $V_2 = 3.15$ µm s⁻¹.

It is interesting to observe that the filtration pressure P_1 , or more precisely the pressure drop from P_1 in the lumen to P=0 at the urinary space, is expended on four sources of resistance along the flow path: entry into the GBM (25% of P_1 , used mostly to compress the gel); Darcy drag within the GBM (17%); exit of the GBM (49%, mostly to counter the buttressing force τ_2 according to equation (2.17)); and the viscous friction as the fluid passes through the SD (9%, according to equation (2.2)). This insight will inform our analysis of the filtration flow through the injured glomerulus in the next section.

We close this section by examining the phenomenon of renal autoregulation. The glomerulus is known for its remarkable ability to maintain a roughly constant GFR despite large variations of the blood pressure [40-43]. Aside from regulation of the afferent arterioles upstream of the glomerulus, Fissel [2] noted that gel compression could be 'an additional mechanism of renal autoregulation of GFR'. To test this idea, we have varied the filtration pressure P_1 in our model and investigated the resultant change in the GFR, represented by the fluid velocity V_1 at the inner boundary of our computational domain ($r = 0.9R_0$). As P_1 increases from the baseline value of 5.3–20 kPa, V_1 increases by only about 61% (figure 6a). This is evidently caused by the progressive compression of the GBM (figure 6b). Kirchheim et al. [40] measured GFR changes in dogs by varying the renal artery pressure, and their data are compared with the model prediction in figure 6a. The model captures the trend of the in vivo data. Thus, 'as pressure-driven flow increases, resistance to further flow increases' [2]. The model confirms

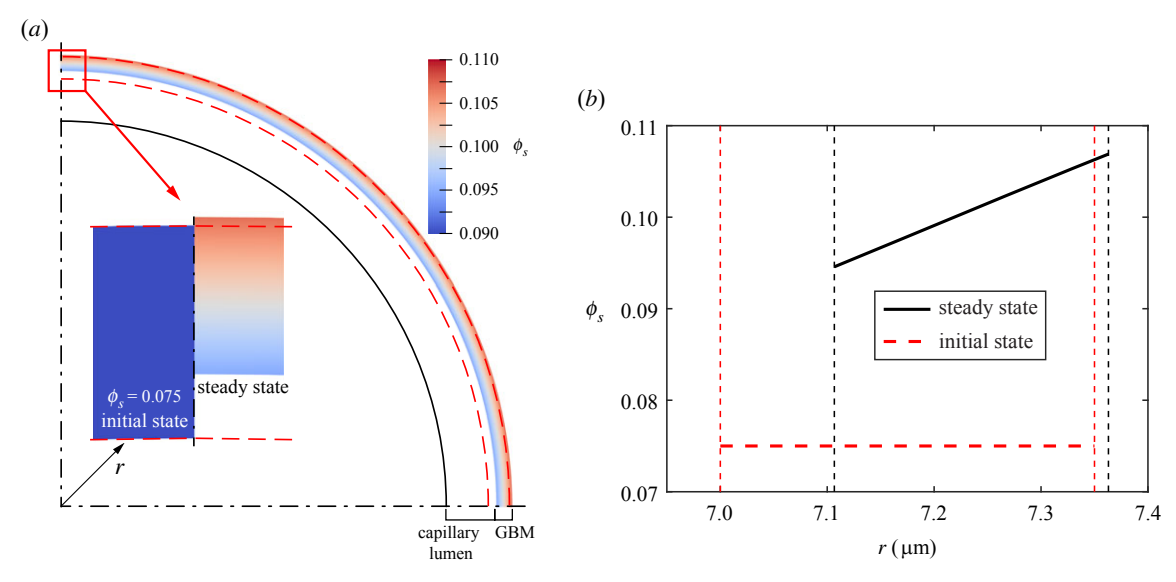


Figure 4. (a) Morphological changes in the GBM due to the filtration flow. The red dashed lines denote the initial edges of the gel layer, and the inset illustrates its displacement and compression. The colour contours represent the solid fraction ϕ_s in the steady compressed state. (b) The steady-state $\phi_s(r)$ profile compared with the initial $\phi_{s0} = 0.075$. The vertical dashed lines mark the location of the gel layer.

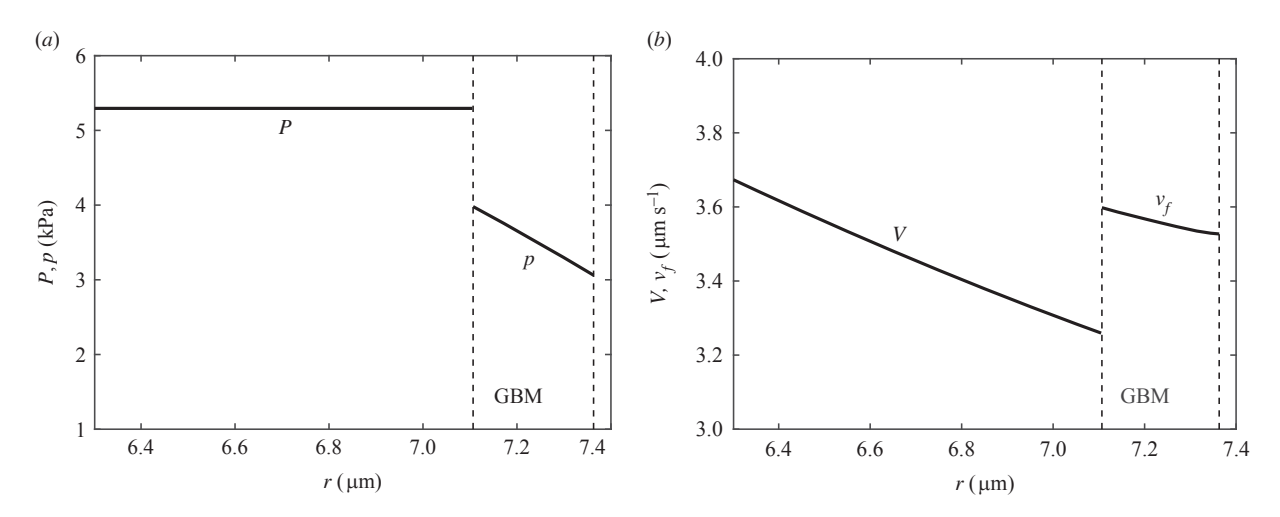


Figure 5. (a) The pressure profiles and (b) the velocity profiles along the radial direction. The vertical dashed lines mark the inner and outer interfaces of GBM.

that gel compression contributes to the autoregulation of glomerular flow.

To sum up the model predictions for the healthy glomerulus, the filtration flow compresses the GBM and increases its solid fraction. Thus, its permeability to large molecules is reduced. This confirms the idea of the gel compression. Next, we use the healthy state as a baseline to investigate the effects of FP injuries.

3.2. The diseased state

Downloaded from https://royalsocietypublishing.org/ on 28 August 2023

As discussed in §2.3, the effacement of the podocyte FPs is modelled through two effects: the softening of the buttressing modulus E, and the constriction of the SD via the friction coefficient μ_D . In the following, we will proceed in two steps. First, we reduce E from the healthy value to the diseased value while keeping μ_D at the healthy value (table 1). Then we increase μ_D to the diseased value.

Figure 7 compares the steady-state solution for the healthy and 'diseased' glomerulus, the latter having a weakened buttress ($E = 2.57 \text{ kPa } \mu\text{m}^{-1}$) but the healthy $\mu_D = 147 \text{ Pa s } \mu\text{m}^{-1}$. First, the most obvious effect of the weakened E is the

pronounced capillary dilatation (figure 7a); the inner radius of the GBM has expanded from 7.11 to 8.41 µm (figure 7b). Second, the capillary dilatation stretches the GBM and makes it thinner. This is clear from figure 7c, where we have aligned the inner surface of the GBM by translating the $\phi_s(r)$ profile for the diseased glomerulus. The GBM thickness has decreased from 0.257 to 0.237 µm. Third, the stretching of the GBM also expands the gel and reduces its solid fraction (figure 7c), thanks to a Poisson ratio v = 0.25 that is below 0.5. Averaged over the GBM thickness, $\bar{\phi}_s$ has decreased by 7%, from 0.10 to 0.093. Finally, as a direct result of the reduced ϕ_s and thinner δ , the GBM presents a lower resistance to filtration, and the GFR has increased by 28% (figure 7b).

These model predictions confirm two features of the gelcompression hypothesis [2,6,8,21]: dilatation of the capillary and increased porosity in the GBM. However, they also contradict two other experimental observations. First, experiments show a lower filtration rate in the injured glomerulus [21,26,44], whereas our model predicts the opposite (figure 7b). Second, GBM thickening is a well-known feature in albuminuria and other glomerular diseases [7,45]. The model predicts GBM thinning (figure 7c).

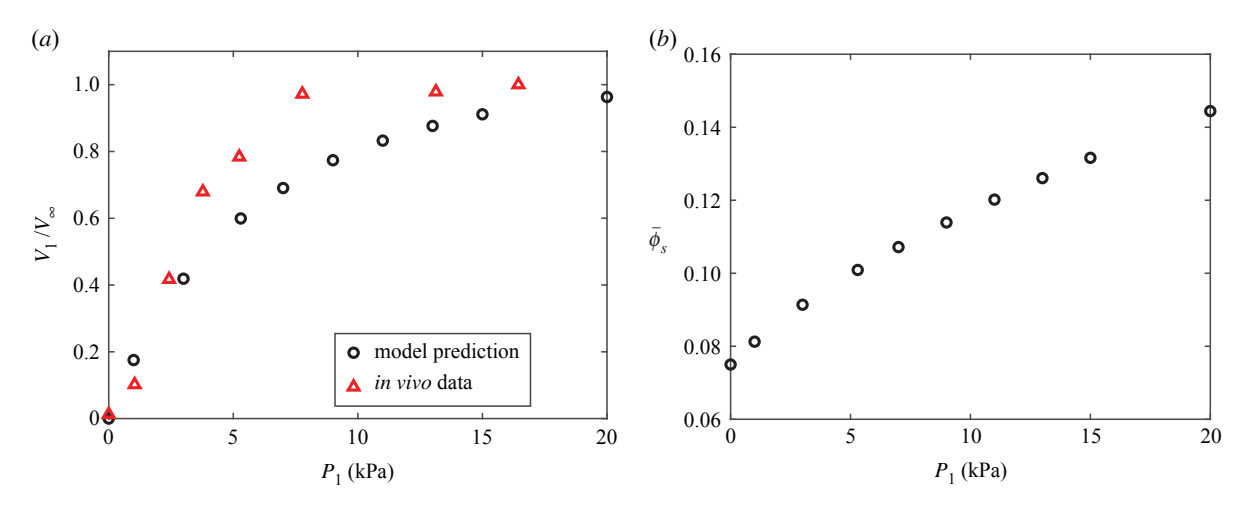


Figure 6. (a) Gel compression causes the filtration flux to plateau at higher filtration pressure P_1 . The fluid velocity V_1 at the inner boundary of the computational domain serves as a convenient proxy for the GFR, and V_{∞} is the plateau value for large P_1 . The model prediction is compared with *in vivo* canine data [40]. (b) The average solid fraction $\overline{\phi}_s$ in the GBM rises with P_1 .

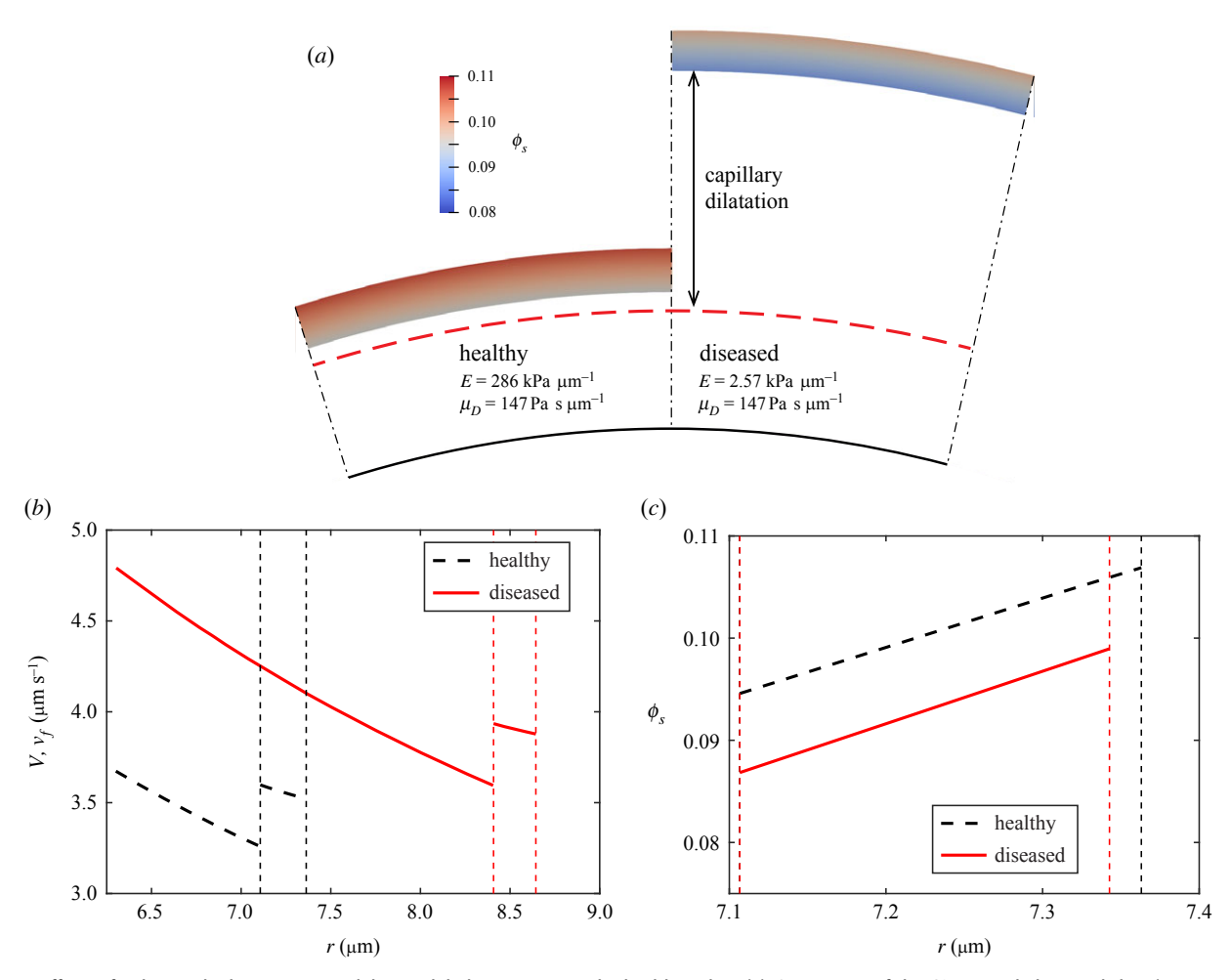


Figure 7. Effects of reducing the buttressing modulus E while keeping μ_D at the healthy value. (a) Comparison of the GBM morphology and the ϕ_S contours. The dashed arc marks the position of the inner boundary of the GBM in the undeformed state. Softening the buttress leads to much greater capillary dilatation. (b) Comparison of the velocity profiles and (c) the solid fraction profiles between the healthy state (black dashed lines) and the diseased state with weakened buttress (solid red lines). The vertical dashed lines mark the boundaries of the GBM layer. In (c), we have shifted the diseased profile to line up its inner radius to that of the healthy profile to facilitate comparison.

The key to resolving these contradictions is the shortening and narrowing of the SD due to FP effacement, another morphological manifestation of podocyte injury. In our model, this is represented by increasing the friction factor μ_D to reflect the constricted area available to the filtrate [21,26,27]. Figure 8 compares the steady-state solutions for the healthy

glomerulus and for a 'diseased' glomerulus with both softened E and elevated μ_D . First, the amount of capillary dilatation is smaller in figure 8a than in figure 7a. Second, the higher μ_D effectively reduces the GFR, which now falls below the healthy solution (figure 8b). Third, the model now predicts a slightly thicker GBM than the healthy solution

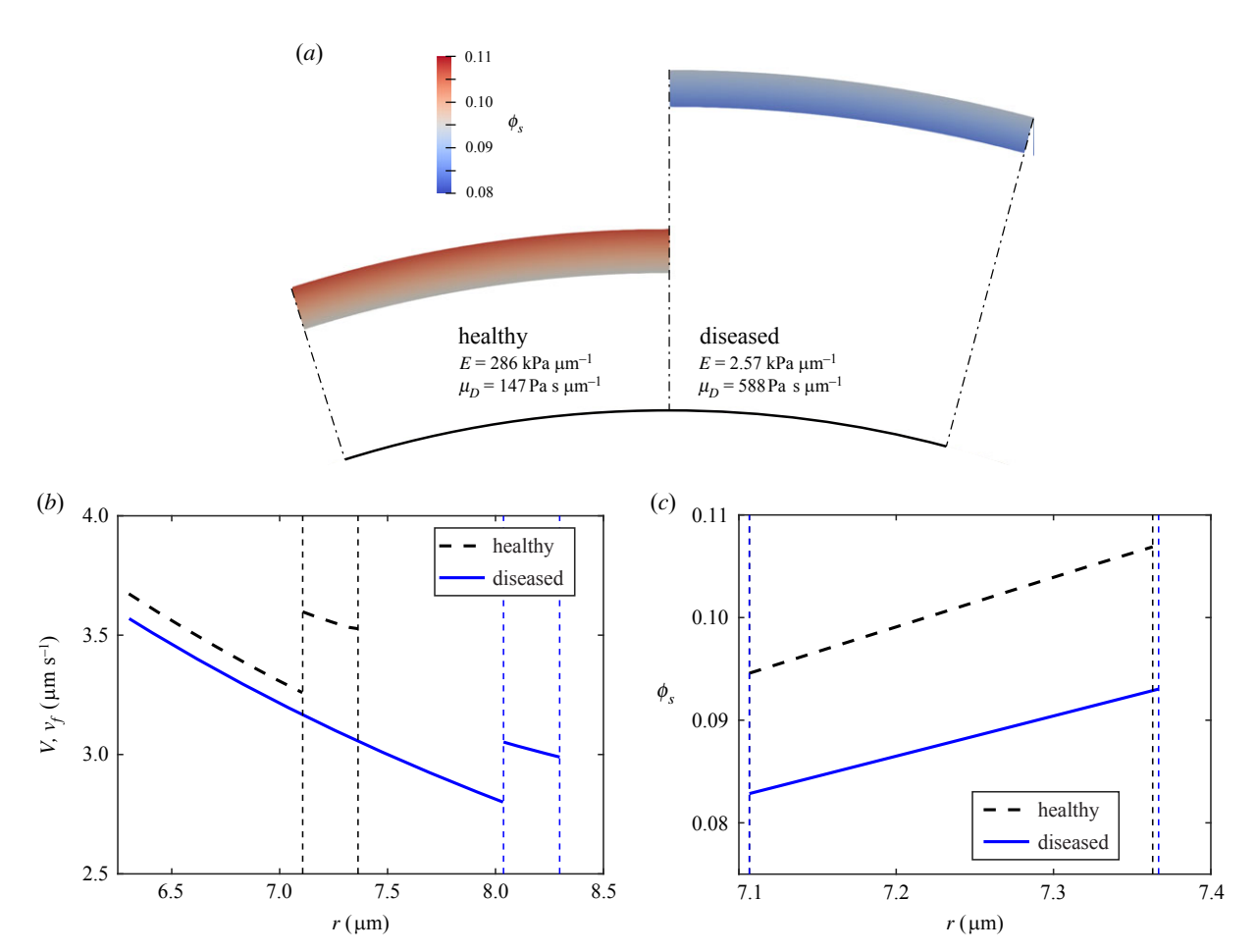


Figure 8. Combined effects of reducing the buttressing modulus E and raising the SD friction coefficient μ_D . (a) Comparison of the GBM morphology and the ϕ_s contours. (b) Comparison of the velocity profiles and (c) the solid fraction profiles between the healthy state (black dashed lines) and the diseased state (solid blue lines). The vertical dashed lines mark the boundaries of the GBM layer. In (c), we have shifted the diseased profile to line up its inner radius to that of the healthy profile to facilitate comparison.

(figure 8c). This is thanks to the reduced GFR; the fluid now exerts a smaller Darcy drag onto the solid network to compress the gel. Thus, including the additional mechanism of SD constriction has resolved the contradictions between figure 7 and *in vivo* observations. Fourth and most interestingly, the GBM becomes even more porous with the raised μ_D ; $\bar{\phi}_s$ is now about 12% below that of the healthy glomerulus. This is again attributable to the decreased flow rate that exerts less compression on the GBM.

The contrast between the healthy and injured state can also be appreciated from how the filtration pressure P_1 is expended on the four sources of resistance. In the diseased state depicted in figure 8, the most notable change is an increase in the resistance of the SD, from 9% of P_1 in the healthy state to 31% in the diseased state. This is at the expense of the other three obstacles: the entry resistance has declined from 25% to 16%, the Darcy drag from 17% to 13%, and the exit resistance from 49% to 40%. These declines are at the root of the smaller capillary dilatation (figure 8a), reduced GFR (figure 8b) and enhanced GBM rarefaction (figure 8c).

In summary, our model predicts that the two pathological consequences of FP effacement, the softening of the buttressing force on the GBM and the reduction of flow area at the SD, each contribute to albuminuria, but through distinct pathways. The weaker buttress allows the GBM to bulge outward and expand its circumference. The constriction of flow area at the SD reduces the GFR, a long-recognized feature of glomeropathy [21,26,44], which in turn reduces the

compaction of the GBM by the interstitial flow. Thus, both conspire to increase the porosity and permeability of the gel. Notably, the thickening of the GBM, which may appear counterintuitive in view of the circumferential stretching of the gel layer, is predicted as a consequence of the suppression of GFR.

4. Discussion

Our initial motivation was to build a mechanical model to test the so-called gel-compression hypothesis [2,6,8], which seeks to explain the onset of albuminuria by the following chain of events:

- (a) Injuries to the FPs of the podocytes cause a loss of buttressing force on the GBM.
- (b) This in turn leads to dilatation of the glomerular capillary under filtration pressure, and circumferential stretching of the GBM.
- (c) The stretching increases the GBM porosity and permeability, allowing proteins to leak from the blood into the urine.

Our model demonstrates how (b) and (c) arise from (a), and thereby confirms the gel-compression hypothesis. In fact, as the GBM is compressed in the healthy state but *expands* in albuminuria, the hypothesis should perhaps be called the 'gel-deformation hypothesis'. Moreover, the model supports the idea that in the healthy glomerulus, gel compression contributes to renal autoregulation of the filtration flux, i.e. the maintenance of a roughly constant flow rate under varying blood pressure.

In comparing the model predictions further with experimental observations [21], we realize that the gel compression and expansion is only part of the story. The other part is the reduction in the GFR by the constriction of available flow area at the SDs, another salient manifestation of FP injury. This is an important mechanical pathway because GFR reduction is a clinical hallmark of albuminuria [26,44]. Moreover, our model has revealed two additional consequences: the lower flow velocity produces less Darcy drag inside the gel, less compression and a secondary reduction in ϕ_s , and it also leads to a thickening of the GBM despite the circumferential stretching.

Therefore, our model not only confirms the gel-deformation hypothesis, but also uncovers the cooperation between two mechanisms: gel expansion due to the weakened FP buttress, and GFR reduction due to SD constriction. Between these two, the model is able to account for all the qualitative trends seen in animal models [21].

Quantitatively, Butt et al. [21] measured the changes in GFR and SD length in a mutant mouse model exhibiting albuminuria, and used a membrane transport model [46] to estimate the increase in hydraulic permeability. Then they were able to back out the required decrease in solid fraction from the Carman-Kozeny equation. Their data imply a reduction of ϕ_s from 0.1 to 0.0864 for two-week-old mutant mice, and further down to 0.0794 for four-week-old mutant mice. Based on the parameter values of table 1, our poroelastic model predicts roughly the same amount of gel expansion; the average solid fraction of the GBM decreases from ϕ_s = 0.10 to 0.088 due to the softening FPs and SD constriction. While Butt et al. deduced the GBM rarefaction in albuminuria from the measured transport, our model goes in the opposite direction: it starts with the poroelastic mechanics of the GBM, and shows that it indeed yields the correct amount of gel expansion under physiological conditions.

In terms of GFR reduction and GBM thickening, the model predicts the correct qualitative trend, but underpredicts the

experimental values of Butt *et al.* [21] by much. The GFR is 30% lower in the mutant mice, whereas the model predicts a 3% decrease (figure 8*b*). The GBM thickens by some 8% *in vivo*, while the model yields a mere 1.5% increase. These two discrepancies are probably related, and the likely causes include the geometric simplifications in the model that disregards any spatial variations along the circumference of the capillary (figure 2), and the uncertainties in evaluating some of the model parameters (table 1).

To conclude, we have built a poroelastic model for the GBM, and used it to study the mechanical factors in the onset of albuminuria. Our main findings are

- The model confirms that effacement of podocyte FPs leads to circumferential stretching of the GBM.
- This increases the porosity of the gel layer, effectively confirming the gel-deformation hypothesis.
- A second mechanism, constriction of the filtration area at the SD, cooperates with the circumferential stretching to further increase GBM porosity.
- Using the best estimates of parameter values, the model reproduces roughly the correct amount of porosity increase in the gel as expected from experimental observations, but underpredicts the reduction in glomerular filtration flux and the magnitude of GBM thickening.

Data accessibility. All data and computer codes are included in the electronic supplementary material [47].

Authors' contributions. Z.X.: conceptualization, data curation, formal analysis, investigation, methodology, software, validation, visualization, writing—original draft, writing—review and editing; P.Y.: data curation, investigation, methodology, software, writing—review and editing; J.J.F.: conceptualization, data curation, funding acquisition, project administration, resources, supervision, writing—original draft, writing—review and editing.

All authors gave final approval for publication and agreed to be held accountable for the work performed therein.

Conflict of interest declaration. We declare we have no competing interests. Funding. J.J.F. was funded by the Natural Sciences and Engineering Research Council of Canada (Discovery grant no. 2019-04162). P.Y. was funded by the National Science Foundation (grant no. DMS-2012480)

Acknowledgements. We thank Leah Keshet, Mattia Bacca and Albert Kong for helpful discussions.

References

Downloaded from https://royalsocietypublishing.org/ on 28 August 2023

- Hausmann R et al. 2010 Electrical forces determine glomerular permeability. J. Am. Soc. Nephrol. 21, 2053–2058. (doi:10.1681/ASN.2010030303)
- Fissell WH. 2020 Reconsidering Garth Robinson: fluid flow and the glomerular filtration barrier. *Curr. Opin. Nephrol. Hypertens.* 29, 273–279. (doi:10. 1097/MNH.0000000000000606)
- Menon MC, Chuang PY, He CJ. 2012 The glomerular filtration barrier: components and crosstalk. *Int. J. Nephrol.* 2012, 749010. (doi:10.1155/2012/749010)
- Tojo A, Kinugasa S. 2012 Mechanisms of glomerular albumin filtration and tubular reabsorption. Int. J. Nephrol. 2012, 481520. (doi:10.1155/2012/ 481520)
- Wilkie M. 2015 Introduction to point-counterpoint: mechanisms of glomerular filtration: pores versus an

- electrical field. *Perit. Dial. Int.* **35**, 4. (doi:10.3747/pdi.2014.00325)
- Fissell WH, Miner JH. 2018 What is the glomerular ultrafiltration barrier? J. Am. Soc. Nephrol. 29, 2262–2264. (doi:10.1681/ASN.2018050490)
- 7. Naylor RW, Morais MRPT, Lennon R. 2021 Complexities of the glomerular basement membrane. *Nat. Rev. Nephrol.* **17**, 112–127. (doi:10.1038/s41581-020-0329-y)
- Benzing T, Salant D. 2021 Insights into glomerular filtration and albuminuria. *N. Engl. J. Med.* 384, 1437–1446. (doi:10.1056/NEJMra1808786)
- Kalluri R. 2006 Proteinuria with and without renal glomerular podocyte effacement. J. Am. Soc. Nephrol. 17, 2383–2389. (doi:10.1681/ASN. 2006060628)

- Garg P. 2018 A review of podocyte biology.
 Am. J. Nephrol. 2018(suppl. 1), 3–13. (doi:10.1159/000481633)
- Sol M, Kamps JA, van der Vlag J, Krenning G, Hillebrands JL. 2020 Glomerular endothelial cells as instigators of glomerular sclerotic diseases. *Front. Pharmacol.* 11, 573557. (doi:10.3389/fphar.2020. 573557)
- 12. Robinson GB, Walton HA. 1989 Glomerular basement membrane as a compressible ultrafilter. *Microvasc. Res.* **38**, 36–48. (doi:10.1016/0026-2862(89)90015-0)
- Smithies O. 2003 Why the kidney glomerulus does not clog: a gel permeation/diffusion hypothesis of renal function. *Proc. Natl Acad. Sci. USA* 100, 4108–4113. (doi:10.1073/pnas.0730776100)

- Grahammer F et al. 2016 A flexible, multilayered protein scaffold maintains the slit in between glomerular podocytes. JCI Insight 1, e86177. (doi:10.1172/jci.insiqht.86177)
- 15. Lawrence MG *et al.* 2017 Permeation of macromolecules into the renal glomerular basement membrane and capture by the tubules. *Proc. Natl Acad. Sci. USA* **114**, 2958–2963. (doi:10.1073/pnas. 1616457114)
- Schlöndorff D, Wyatt CM, Campbell KN. 2017 Revisiting the determinants of the glomerular filtration barrier: what goes round must come round. Kidney Int. 92, 533–536.
- Rippe B, Haraldsson B. 1994 Transport of macromolecules across microvascular walls: the twopore theory. *Physiol. Rev.* 74, 163–219. (doi:10. 1152/physrev.1994.74.1.163)
- Rippe B, Öberg CM. 2015 Counterpoint: defending pore theory. *Perit. Dial. Int.* 35, 9–13. (doi:10.3747/ pdi.2014.00110)
- Moeller MJ, Kuppe C. 2015 Point: proposing the electrokinetic model. *Perit. Dial. Int.* 35, 5–8. (doi:10.3747/pdi.2014.00189)
- Lazzara MJ, Deen WM. 2007 Model of albumin reabsorption in the proximal tubule. *Am. J. Physiol. Ren. Physiol.* 292, F430–F439. (doi:10.1152/ ajprenal.00010.2006)
- 21. Butt L *et al.* 2020 A molecular mechanism explaining albuminuria in kidney disease. *Nat. Metab.* **2**, 461–474. (doi:10.1038/s42255-020-0204-y)
- Kriz W, Hackenthal E, Nobiling R, Sakai T, Elger M, Hähnel B. 1994 A role for podocytes to counteract capillary wall distension. *Kidney Int.* 45, 369–376. (doi:10.1038/ki.1994.47)

Downloaded from https://royalsocietypublishing.org/ on 28 August 2023

- Li H, Zheng Y, Han YL, Cai S, Guo M. 2021
 Nonlinear elasticity of biological basement membrane revealed by rapid inflation and deflation. Proc. Natl Acad. Sci. USA 118, e2022422118. (doi:10.1073/pnas.2022422118)
- Khalilgharibi N, Mao Y. 2021 To form and function: on the role of basement membrane mechanics in tissue development, homeostasis and disease. *Open Biol.* 11, 200360. (doi:10.1098/rsob.200360)
- Li L, Zhang J, Xu Z, Young YN, Feng JJ, Yue P. 2022
 An arbitrary Lagrangian-Eulerian method for simulating interfacial dynamics between a hydrogel

- and a fluid. *J. Comput. Phys.* **451**, 110851. (doi:10. 1016/j.jcp.2021.110851)
- Drumond MC, Kristal B, Myers BD, Deen WM. 1994 Structural basis for reduced glomerular filtration capacity in nephrotic humans. *J. Clin. Invest.* 223, 1187–1195. (doi:10.1172/JC1117435)
- Wartiovaara J et al. 2004 Nephrin strands contribute to a porous slit diaphragm scaffold as revealed by electron tomography. J. Clin. Invest. 114, 1475–1483. (doi:10.1172/JCl22562)
- Beris AN, Horner JS, Jariwala S, Armstrong MJ, Wagner NJ. 2021 Recent advances in blood rheology: a review. Soft Matter 17, 10 591–10 613. (doi:10.1039/D1SM01212F)
- 29. Feng JJ, Young YN. 2020 Boundary conditions at a gel-fluid interface. *Phys. Rev. Fluids* **5**, 124304. (doi:10.1103/PhysRevFluids.5.124304)
- Arndt D *et al.* 2021 The deal.II library, Version 9.3.
 J. Numer. Math. 29, 171–186. (doi:10.1515/jnma-2021-0081)
- Terasaki M, Brunson JC, Sardi J. 2020 Analysis of the three dimensional structure of the kidney glomerulus capillary network. *Sci. Rep.* 10, 20334. (doi:10.1038/s41598-020-77211-x)
- Nader E et al. 2019 Blood rheology: key parameters, impact on blood flow, role in sickle cell disease and effects of exercise. Front. Physiol. 10, 1329. (doi:10. 3389/fphys.2019.01329)
- Késmárky G, Kenyeres P, Rábai M, Tóth K. 2008 Plasma viscosity: a forgotten variable. Clin. Hemorheol. Microcirc. 39, 243–246.
- Inman BA et al. 2013 The impact of temperature and urinary constituents on urine viscosity and its relevance to bladder hyperthermia treatment. Int. J. Hyperthermia 29, 206–210. (doi:10.3109/ 02656736.2013.775355)
- Last JA, Liliensiek SJ, Nealey PF, Murphy CJ. 2009
 Determining the mechanical properties of human
 corneal basement membranes with atomic force
 microscopy. *J. Struct. Biol.* 167, 19–24. (doi:10.
 1016/j.jsb.2009.03.012)
- Klaentschi K, Brown JA, Niblett PG, Shore AC, Tooke JE. 1998 Pressure-permeability relationships in basement membrane: effects of static and dynamic pressures. Am. J. Physiol. Heart. Circ. Physiol. 274, H1327—H1334. (doi:10.1152/ajpheart.1998.274.4. H1327)

- Rodewald R, Karnovsky MJ. 1974 Porous substructure of the glomerular slit diaphragm in the rat and mouse. J. Cell Biol. 60, 423–433.
- Gagliardini E, Conti S, Benigni A, Remuzzi G, Remuzzi A. 2010 Imaging of the porous ultrastructure of the glomerular epithelial filtration slit. J. Am. Soc. Nephrol. 21, 2081–2089. (doi:10. 1681/ASN.2010020199)
- Rice WL, Van Hoek AN, Punescu TG, Huynh C, Goetze B, Singh B, Scipioni L, Stern LA, Brown D. 2013 High resolution helium ion scanning microscopy of the rat kidney. *PLoS ONE* 8, e57051. (doi:10.1371/journal.pone.0057051)
- Kirchheim HR, Ehmke H, Hackenthal E, Löwe W, Persson P. 1987 Autoregulation of renal blood flow, glomerular filtration rate and renin release in conscious dogs. *Pflüg. Arch.* 410, 441–449. (doi:10. 1007/BF00586523)
- Layton AT, Edwards A. 2014 Mathematical modeling in renal physiology. Berlin, Germany: Springer. (doi:10.1007/978-3-642-27367-4)
- 42. Sgouralis I, Layton AT. 2015 Mathematical modeling of renal hemodynamics in physiology and pathophysiology. *Math. Biosci.* **264**, 8–20. (doi:10. 1016/j.mbs.2015.02.016)
- Carlström M, Wilcox CS, Arendshorst WJ. 2015 Renal autoregulation in health and disease. *Physiol. Rev.* 95, 405–511. (doi:10.1152/physrev.00042.2012)
- Shemesh O, Ross JC, Deen WM, Grant GW, Myers BD. 1986 Nature of the glomerular capillary injury in human membranous glomerulopathy. J. Clin. Invest. 77, 868–877. (doi:10.1172/ JCI112384)
- Butt L, Unnersjo-Jess D, Hohne M, Schermer B, Edwards A, Benzing T. 2021 A mathematical estimation of the physical forces driving podocyte detachment. *Kidney Int.* **100**, 1054–1062. (doi:10. 1016/j.kint.2021.06.040)
- Edwards A, Daniels BS, Deen WM. 1997 Hindered transport of macromolecules in isolated glomeruli.
 II. Convection and pressure effects in basement membrane. *Biophys. J.* 72, 214–222. (doi:10.1016/S0006-3495(97)78660-0)
- Xu Z, Yue P, Feng JJ. 2023 Poroelastic modelling reveals the cooperation between two mechanisms for albuminuria. Figshare. (doi:10.6084/m9.figshare. c.6350499)